Supplementary Materials for

Tuning T cell receptor sensitivity through catch bond engineering

Xiang Zhao, Elizabeth M. Kolawole, Waipan Chan, Yinnian Feng, Xinbo Yang, Marvin Gee, Kevin M. Jude, Leah V. Sibener, Polly M. Fordyce, Ronald N. Germain, Brian D. Evavold, K. Christopher Garcia*

*Corresponding author. Email: kcgarcia@stanford.edu

This PDF file includes:

Figs. S1 to S16

Tables S1 to S12

Supplementary Figure 1

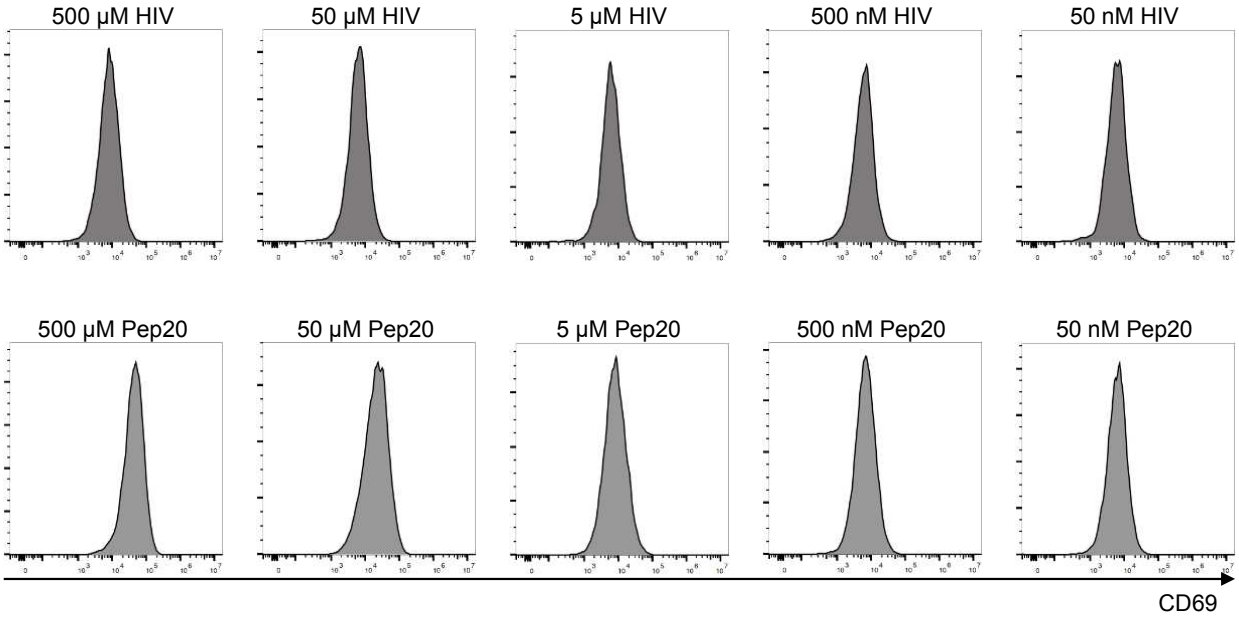

Figure S1. Representative flow cytometry plots of Figure 1A.

Supplementary Figure 2

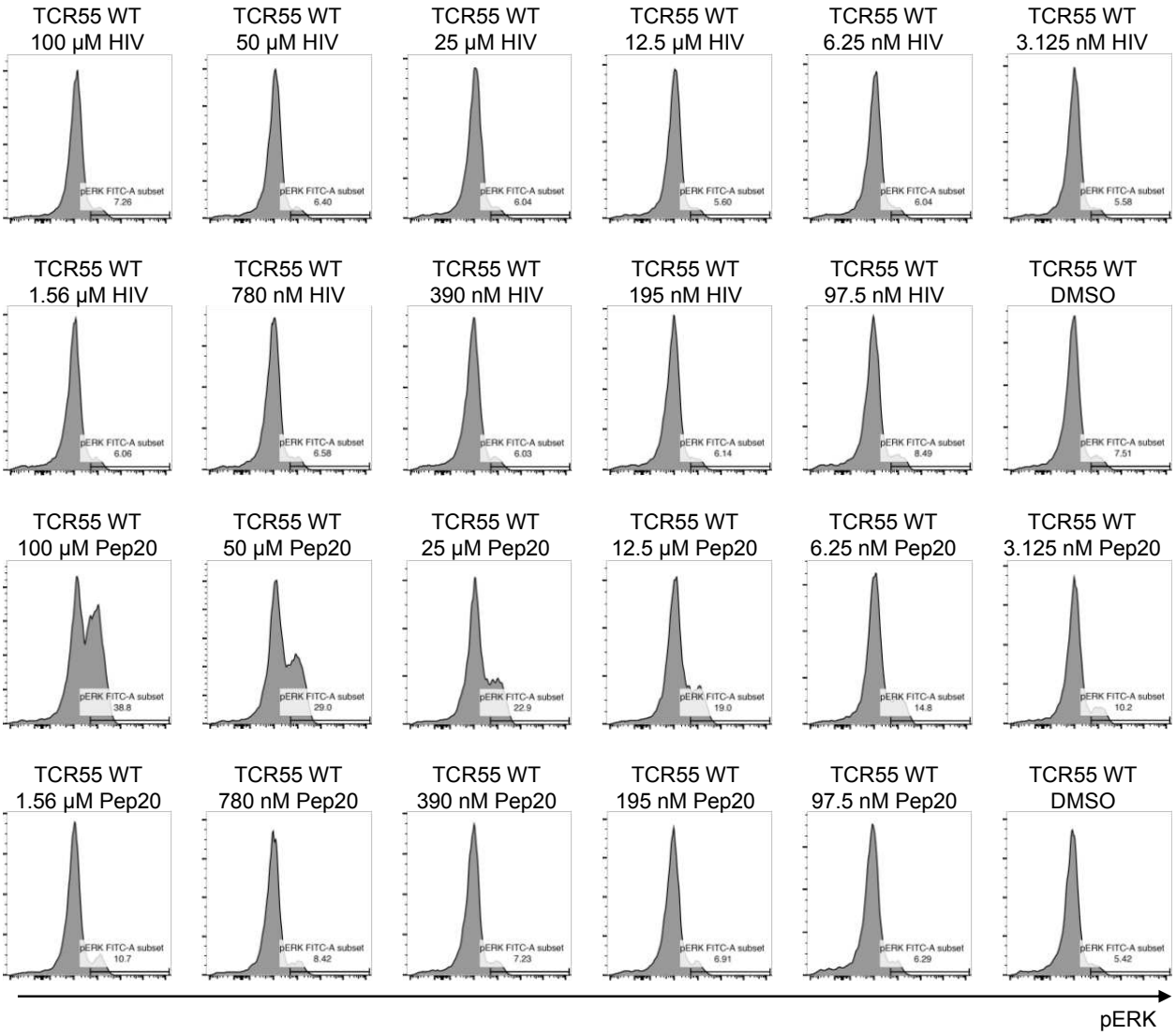

Figure S2. Representative flow cytometry plots of Figure 1B.

Supplementary Figure 3

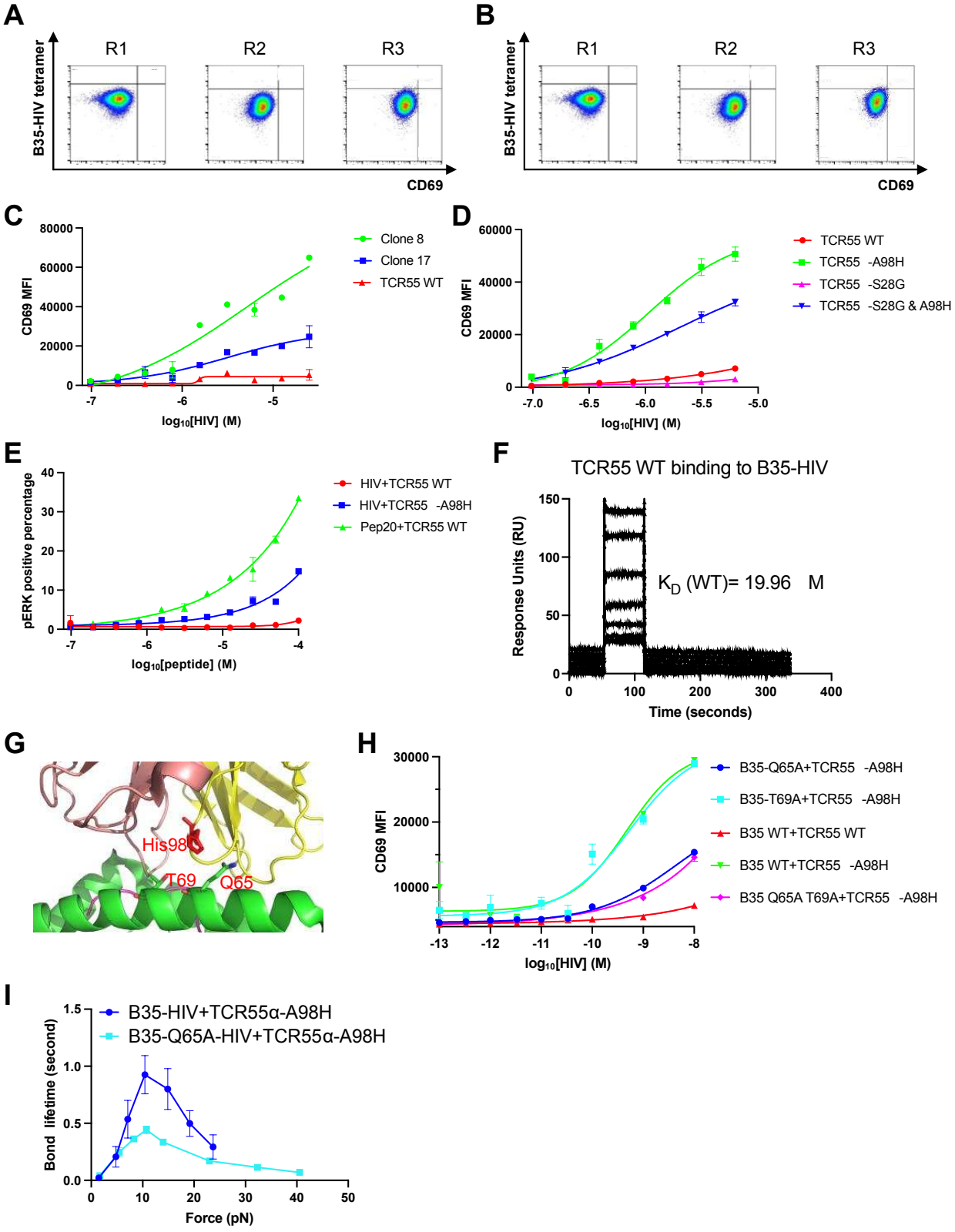

Figure S3. Deconvolution of stimulatory TCR55α-A98 mutants.

(A) B35-HIV tetramer staining and anti-CD69 staining of TCR55 WT SKW3 transfectants in each round of selection of Vα library.

(B) B35-HIV tetramer staining and anti-CD69 staining of TCR55 WT SKW3 transfectants in each round of selection of Vβ library.

(C) Clone 8, clone 17 and TCR55 WT SKW3 T cell transfectants were stimulated by KG-1 cells pulsed with titrated HIV peptide. Anti-CD69 staining of T cells was performed and analyzed by flow cytometry.

(D) TCR55α-S28G A98H, TCR55α-S28G, TCR55α-A98H were transduced with WT TCR55β in SKW3 T cells and the transfectants were stimulated by KG-1 cells pulsed with titrated HIV peptide. Anti-CD69 staining of T cells was performed and analyzed by flow cytometry.

(E) TCR55 or TCR55α-A98H-transduced SKW3 T cells were stimulated by KG-1 cells pulsed with titrated HIV or Pep20 peptides for 15 min. Anti-phospho-ERK staining was performed on the SKW3 T cells and analyzed by flow cytometry.

(F) SPR measurement of TCR55 WT protein binding to B35-HIV. Biotinylated B35-HIV monomer was immobilized on the streptavidin chip and the TCR55 WT protein was flowed through the chip.

(G) Zoomed view of B35-HIV-TCR55 structure with mutagenesis of TCR55α-A98H modeled with Pymol.

(H) B35-T69A, B35-Q65A, B35-Q65A T69A effects on TCR55α-A98H activation. Different B35 mutants were transduced into K562 cells. K562 transfectants were used as antigen-presenting cells to be pulsed with titrated HIV peptide and then stimulate different SKW3 T cell transfectants. Anti-CD69 staining of T cells was performed and analyzed by flow cytometry.

(I) Biomembrane force probe experiments to measure bond lifetime force curves for TCR55α-A98H binding to B35-Q65A-HIV. Data are shown as mean ± SEM of 500+ individual bond lifetimes per force curve.

(C-E, H) Data are representative of 3 independent experiments. Data are shown as mean ± SD of technical triplicates.

Supplementary Figure 4

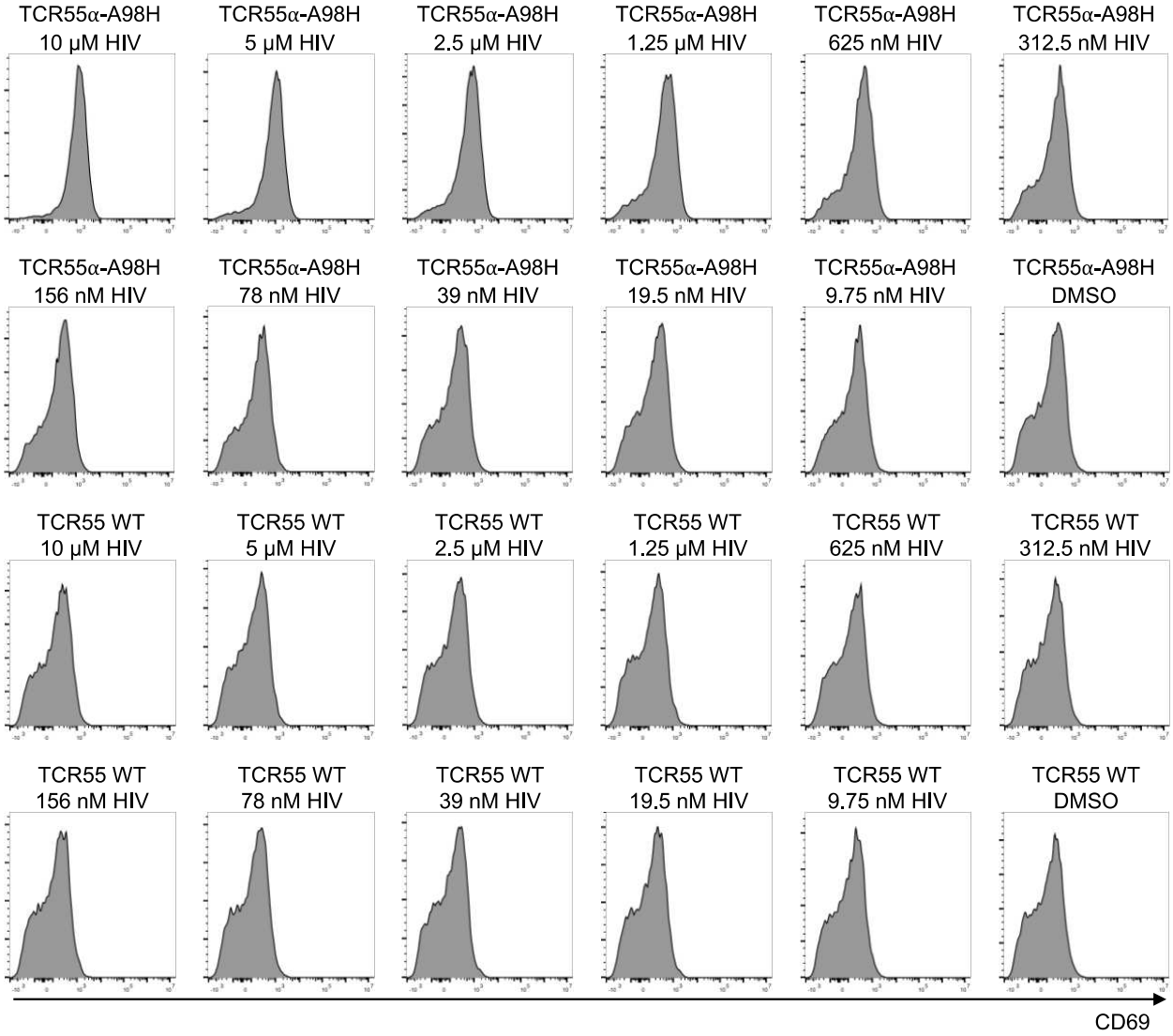

Figure S4. Representative flow cytometry plots of Figure 2B.

Supplementary Figure 5

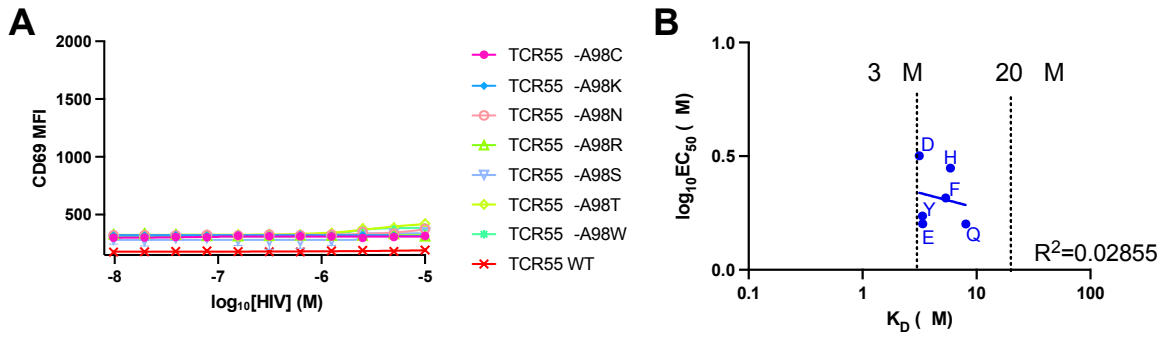

Figure S5. Non-stimulatory TCR55α-A98 mutants, and the correlation between EC_{50} and 3D binding affinity K_D of stimulatory TCR55α-A98 mutants.

(A) TCR55α-A98 was mutated to C, K, N, R, S, T, and W and used to transduce SKW3 T cells with WT TCR55β. The transfectants were stimulated by KG-1 cells pulsed with titrated HIV peptides for 14 hours. Anti-CD69 staining was performed on the SKW3 T cells and analyzed by flow cytometry.

(B) $log_{10}EC_{50}$ versus 3D binding affinity K_D of stimulatory TCR55α-A98 mutants transfectants.

(A) Data are representative of 3 independent experiments. Data are shown as mean ± SD of technical triplicates.

Supplementary Figure 6

A

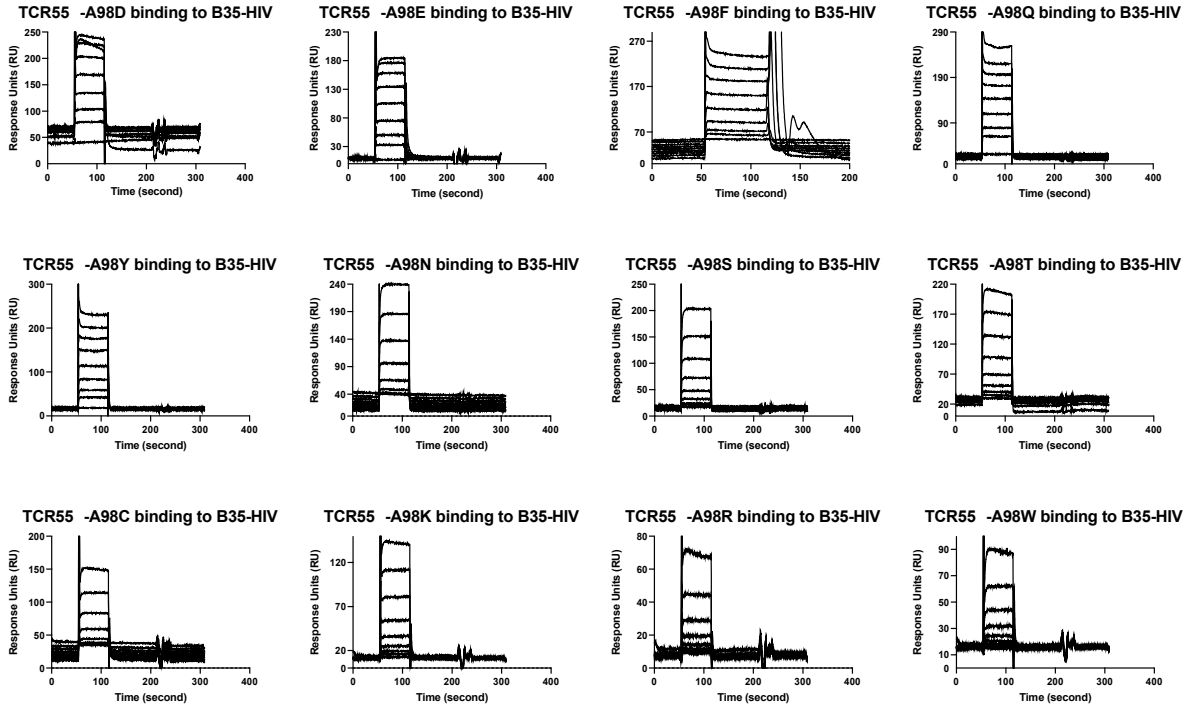

B

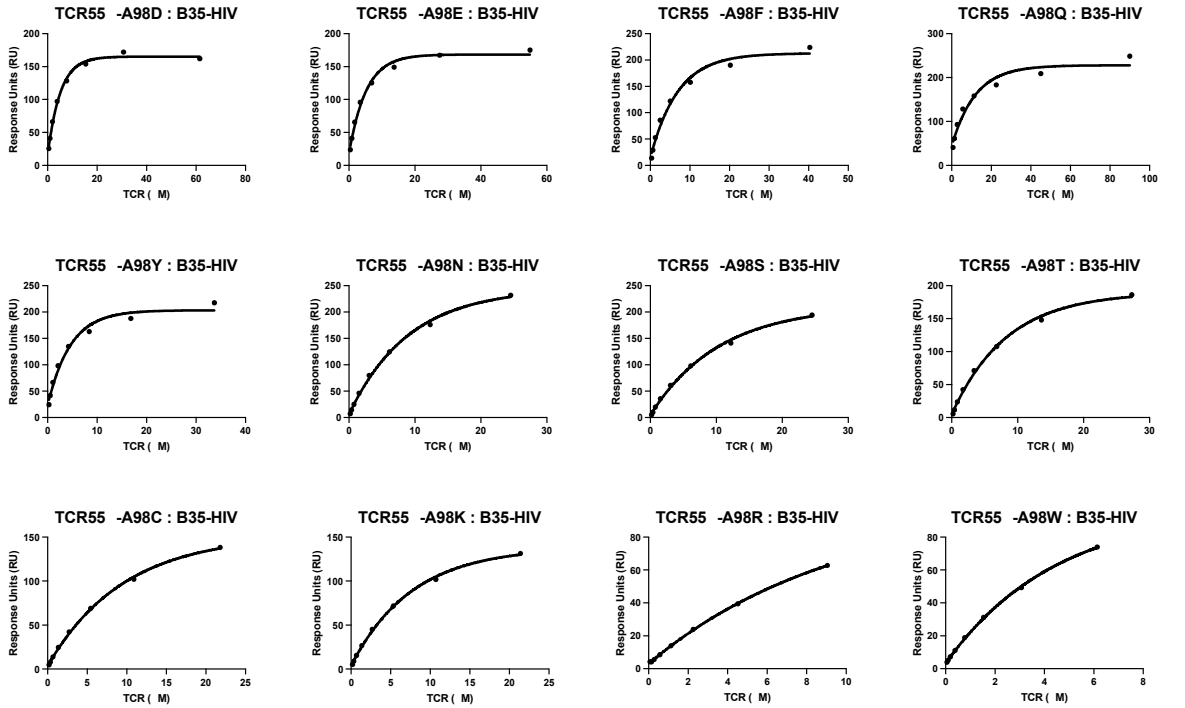

Figure S6. SPR experiments of TCR55α-A98 mutants.

(A) SPR measurement of TCR55α-A98 mutants protein binding to B35-HIV. Biotinylated B35-HIV monomer was immobilized on the streptavidin chip and the TCR55α-A98 mutant proteins were flowed through the chip.

(B) Determination of 3D affinity between TCR55α-A98 mutants and B35-HIV by SPR. Equilibrium curves of TCR55α-A98 mutants binding to B35-HIV pMHC at 25°C. Data shown were measured at equilibrium (black dots). Black lines show the fit to a 1:1 binding curve.

Supplementary Figure 7

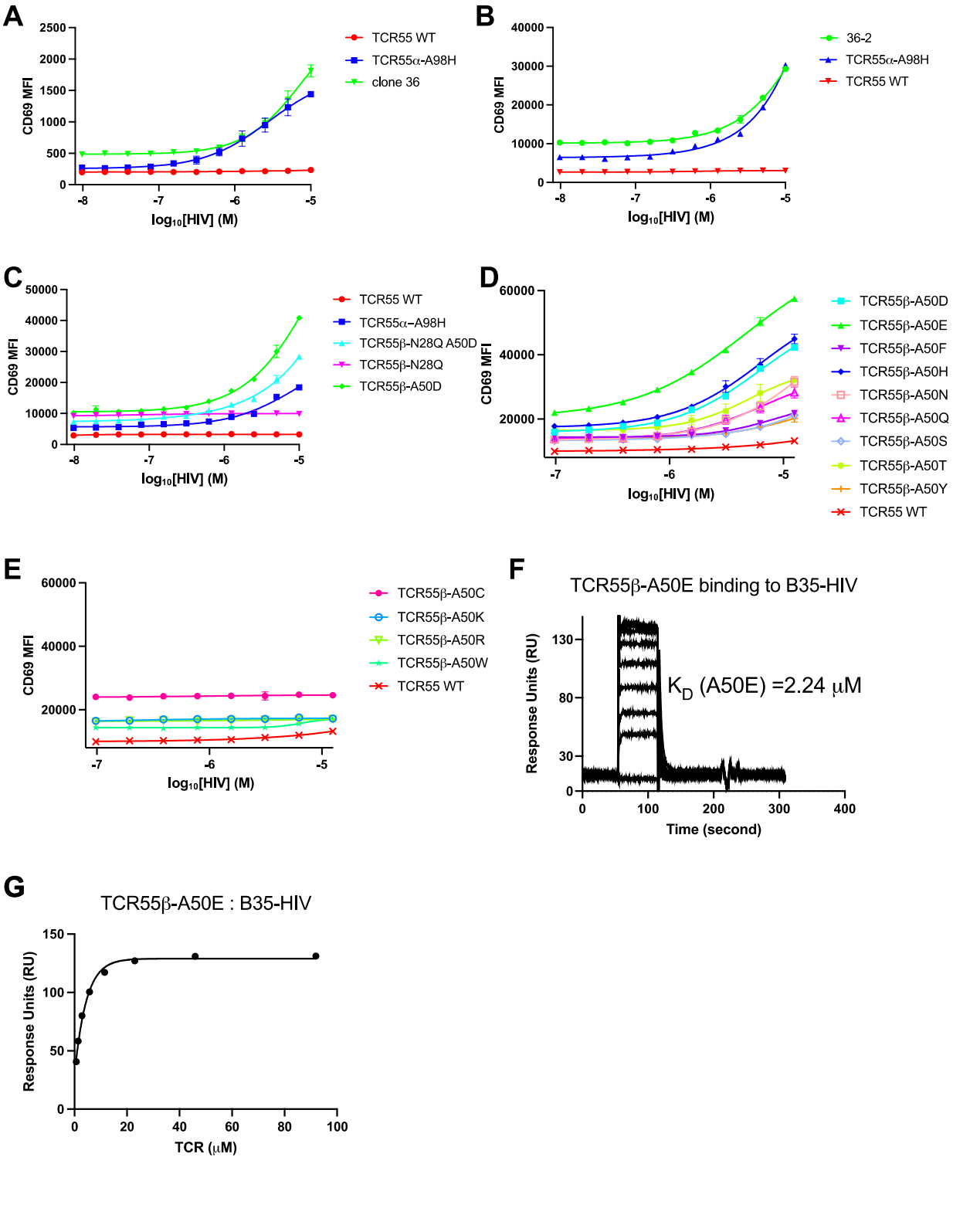

Figure S7. Deconvolution of stimulatory TCR55β-A50 mutants.

(A) Clone 36 from Vβ library was tested along with TCR55 WT and TCR55α-A98H mutant. The T cell transfectants were stimulated by KG-1 cells pulsed with titrated HIV peptide. Anti-CD69 staining of T cells was performed and analyzed by flow cytometry.

(B) The TCR 36-2 sequenced from clone 36 was transduced in SKW3 T cells and the transfectants were stimulated by KG-1 cells pulsed with titrated HIV peptide. Anti-CD69 staining of T cells was performed and analyzed by flow cytometry.

(C) The TCR55β-N28Q A50D, TCR55β-N28Q, TCR55β-A50D were transduced with WT TCR55α in SKW3 T cells and the transfectants were stimulated by KG-1 cells pulsed with titrated HIV peptide. Anti-CD69 staining of T cells was performed and analyzed by flow cytometry.

(D) The TCR55β-A50 was mutated to D, E, F, H, N, Q, S, T, and Y. The TCR55β-A50 mutants were transduced with WT TCR55α in SKW3 T cells and the transfectants were stimulated by KG-1 cells pulsed with titrated HIV peptide. Anti-CD69 staining of T cells was performed and analyzed by flow cytometry.

(E) The TCR55β-A50 was mutated to C, K, R, and W. The TCR55β-A50 mutants were transduced with WT TCR55α in SKW3 T cells and the transfectants were stimulated by KG-1 cells pulsed with titrated HIV peptide. Anti-CD69 staining of T cells was performed and analyzed by flow cytometry.

(F) SPR experiments of TCR55β-A50E protein binding to B35-HIV. Biotinylated B35-HIV monomer was immobilized on the streptavidin chip and the TCR55β-A50E proteins were flowed through the chip.

(G) Determination of 3D affinity between TCR55β-A50E and B35-HIV by SPR. Equilibrium curves of TCR55β-A50E mutants binding to B35-HIV pMHC at 25°C. Data shown was measured at equilibrium (black dots). Black lines show the fit to a 1:1 binding curve.

(A-E) Data are representative of 3 independent experiments. Data are shown as mean ± SD of technical triplicates.

Supplementary Figure 8

A

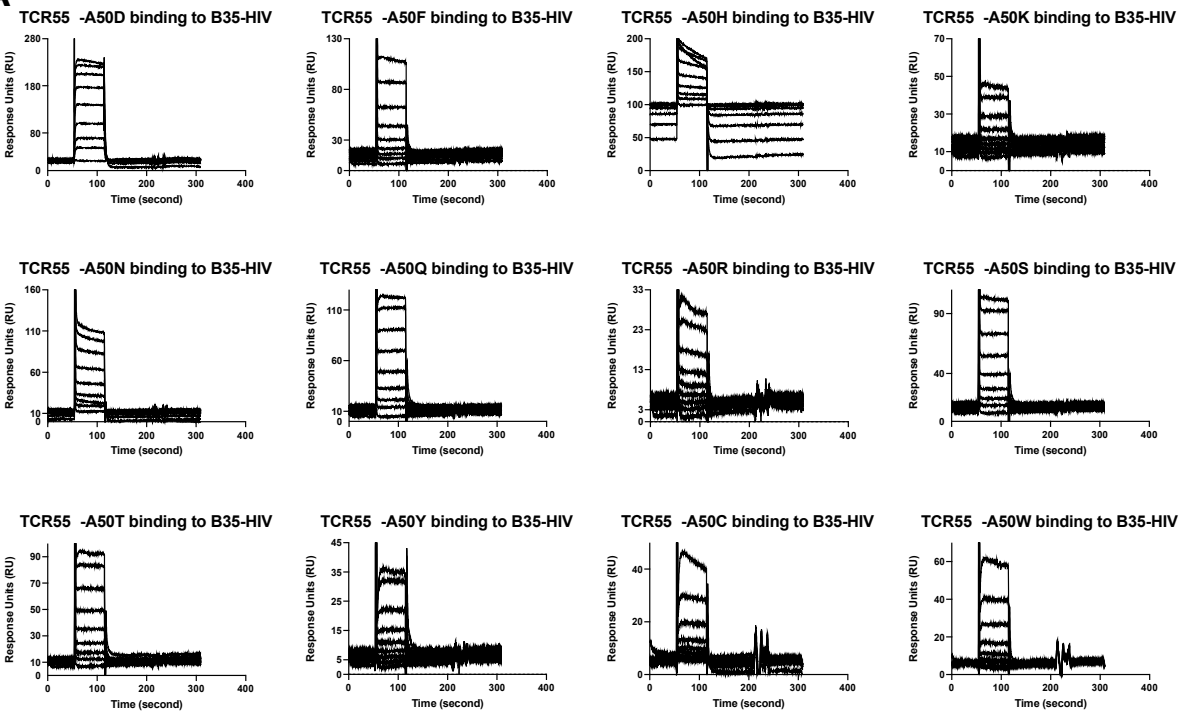

B

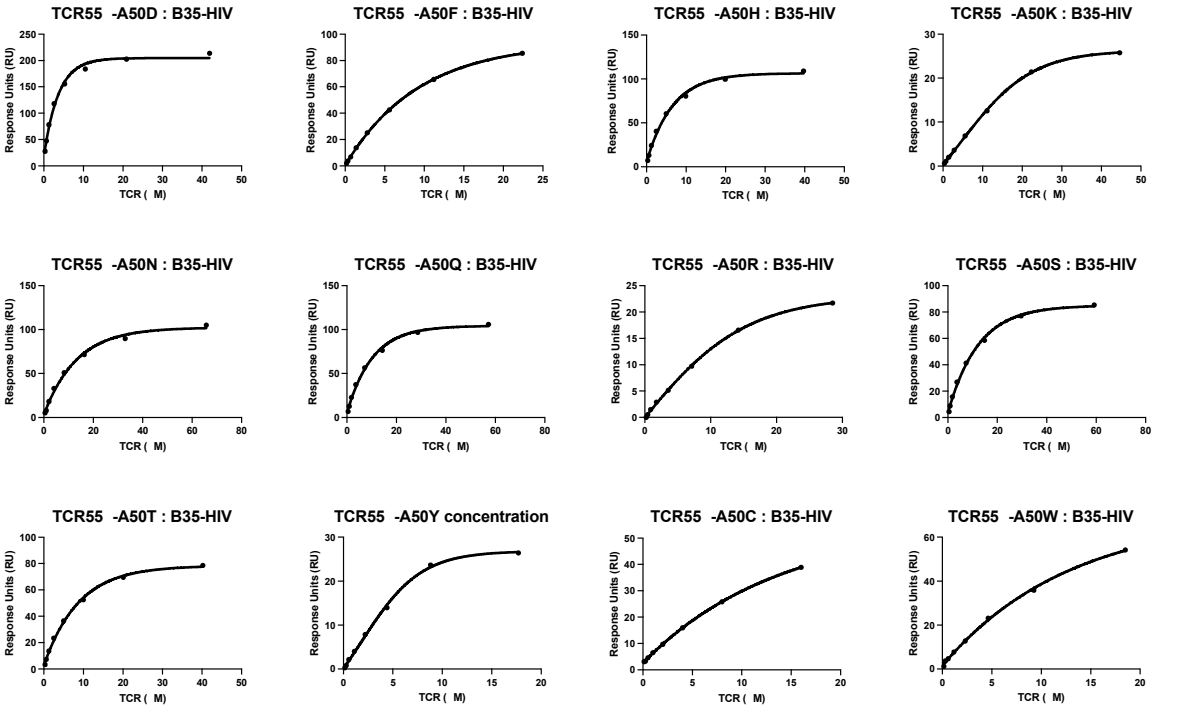

Figure S8. SPR experiments of TCR55β-A50 mutants.

(A) SPR experiments of TCR55β-A50 mutants protein binding to B35-HIV. Biotinylated B35-HIV monomer was immobilized on the streptavidin chip and the TCR55β-A50 mutant proteins were flowed through the chip.

(B) Determination of 3D affinity between TCR55β-A50 mutants and B35-HIV by SPR. Equilibrium curves of TCR55β-A50 mutants binding to B35-HIV pMHC at 25°C. Data shown were measured at equilibrium (black dots). Black lines show the fit to a 1:1 binding curve.

Supplementary Figure 9

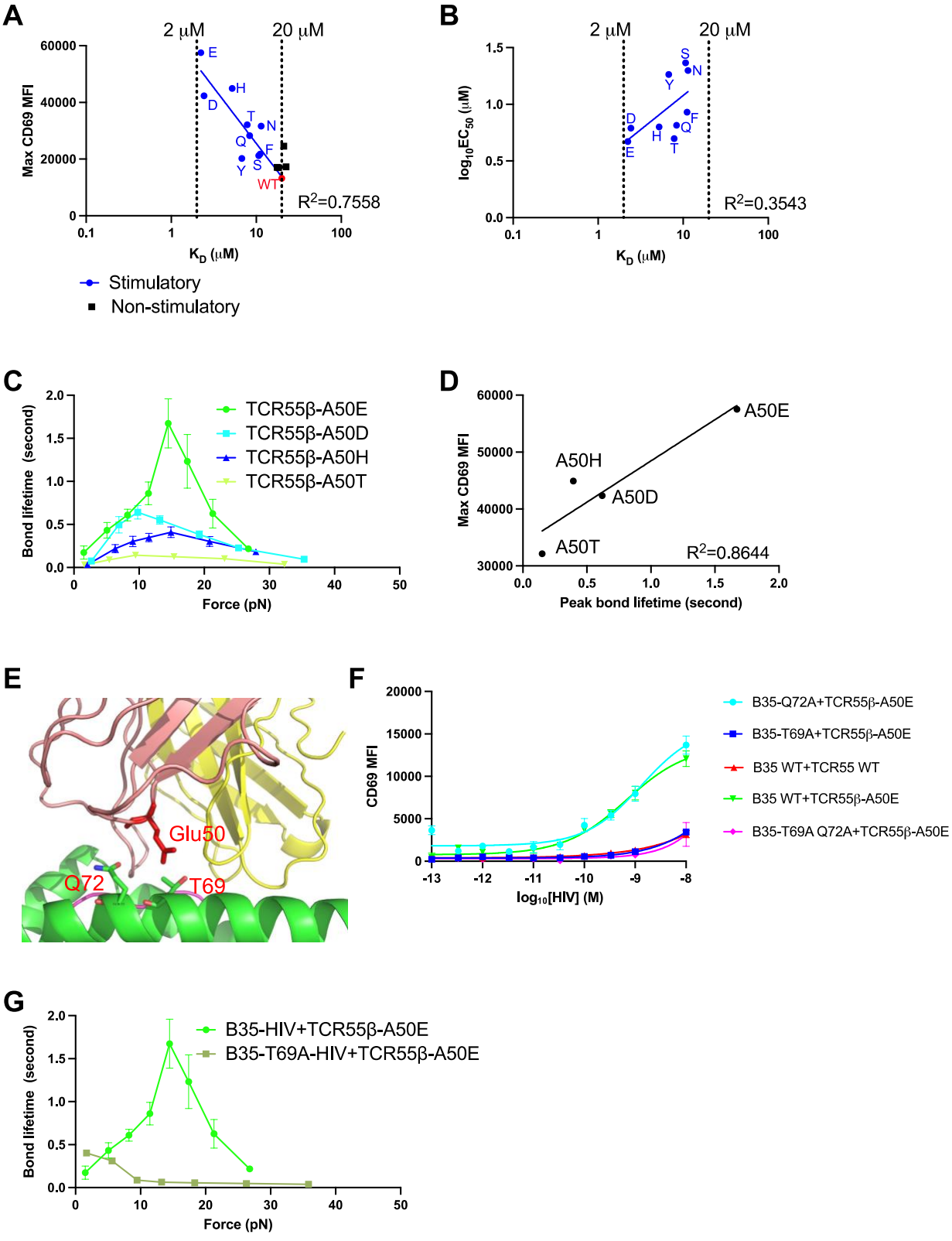

Figure S9. Tuning TCR signaling strength of TCR55β-A50 mutants by different level of catch bonds.

(A) Mean value of maximal anti-CD69 MFI versus 3D binding affinity K_D of TCR55β-A50 mutants. A linear correlation analysis was performed for stimulatory mutants and TCR55 WT.

(B) $\log_{10}EC_{50}$ versus 3D binding affinity K_D of stimulatory TCR55β-A50 mutants

(C) Biomembrane force probe experiments to measure bond lifetime force curves for TCR55β-A50E, TCR55β-A50D, TCR55β-A50H or TCR55β-A50T binding to B35-HIV. Data are shown as mean ± SEM of 500+ individual bond lifetimes per force curve.

(D) Mean value of maximal anti-CD69 MFI versus peak bond lifetime for TCR55β-A50 mutants.

(E) Zoomed view of B35-HIV-TCR55 structure with mutagenesis of TCR55β-A50E modeled with Pymol.

(F) B35-T69A, B35-Q72A, B35-T69A Q72A effects on TCR55β-A50E activation. Different B35 mutants were transduced into K562 cells. K562 transfectants were used as antigen-presenting cells pulsed with titrated HIV peptide and then used to stimulate different SKW3 T cell transfectants. Anti-CD69 staining of T cells was performed and analyzed by flow cytometry. Data are representative of 3 independent experiments. Data are shown as mean ± SD of technical triplicates.

(G) Biomembrane force probe experiments to measure bond lifetime force curves for TCR55β-A50E binding to B35-T69A-HIV. Data are shown as mean ± SEM of 500+ individual bond lifetimes per force curve.

Supplementary Figure 10

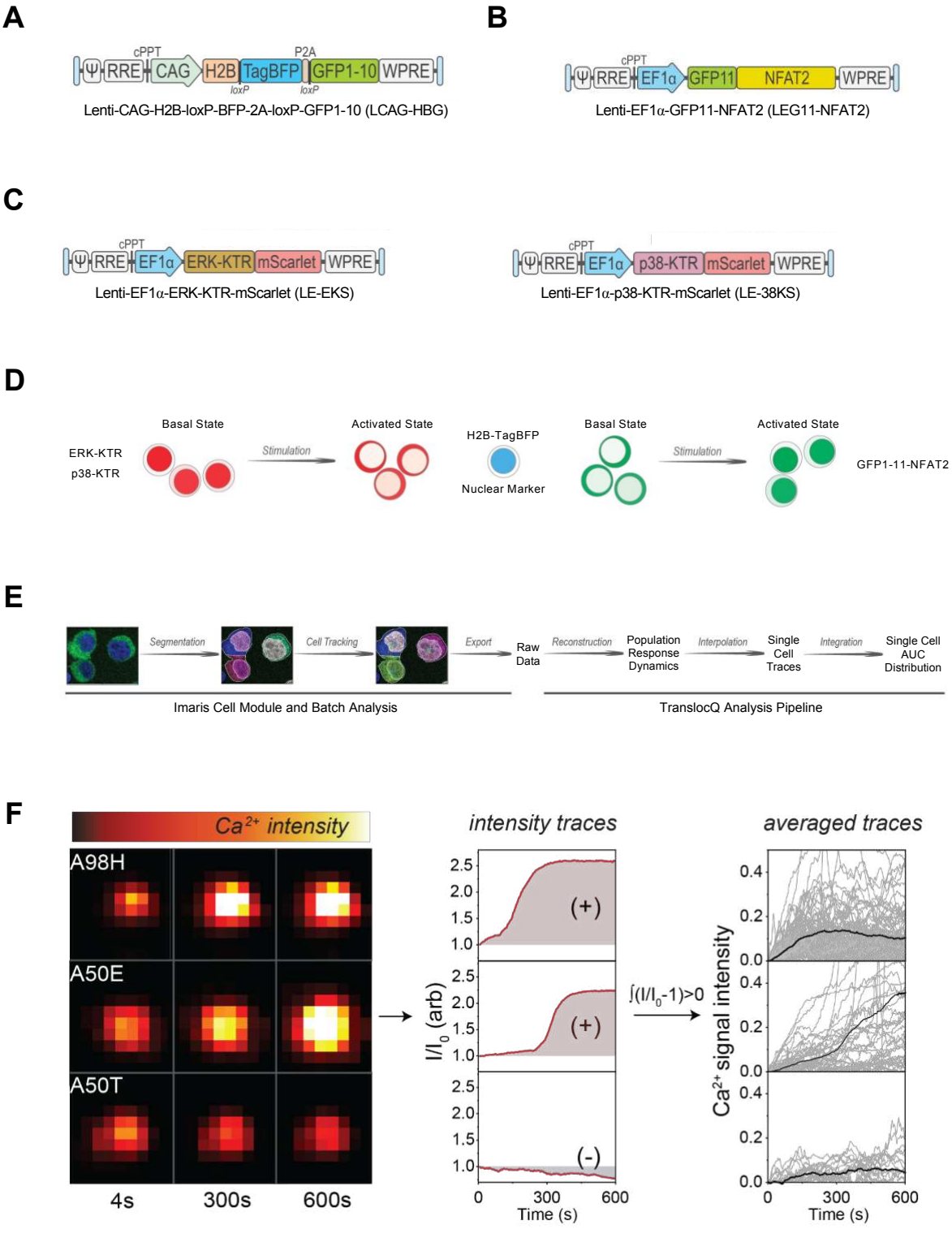

Figure S10. Quantitative live cell imaging analysis of ERK, NFAT2 and p38 signaling dynamics and illustration of BATTLES.

(A) H2B-tBFP nuclear marker expression and split-GFP complementation reporter system LCAG-HBG.

(B) LEG11-NFAT2 lentiviral vector for EF1α promoter driven GFP11-NFAT2 expression.

(C) Lentiviral vector LE-EKS or LE-38KS for stable expression of ERK or p38 kinase translocation reporter (KTR).

(D) Schematic diagram of Jurkat live cell imaging reporter translocation states.

(E) Live cell confocal time-lapse fluorescence microscopy data analysis using Imaris Cell module and TranslocQ pipelines.

(F) Representative images (left) and processed intensity traces (middle) quantifying Ca^{2+} flux within single TCR55 mutants T cells interacting with pMHC-coated thermo-responsive beads bearing the stimulatory HIVpol peptide (IPLTEEAEL). Ca^{2+} flux signals of each single cells are indicated as the ratio of fluorescence intensity (I) at a certain time to the initial fluorescence intensity (I0) of the Ca^{2+}-sensitive dye. The “+” and “-” indicates the positive and negative integrated signals over time. Right: Ca^{2+} signal intensity as a function of time for all positive single cells ($\int(I/I0-1) > 0$) (light grey); mean signal intensity over time is shown in black.

Supplementary Figure 11

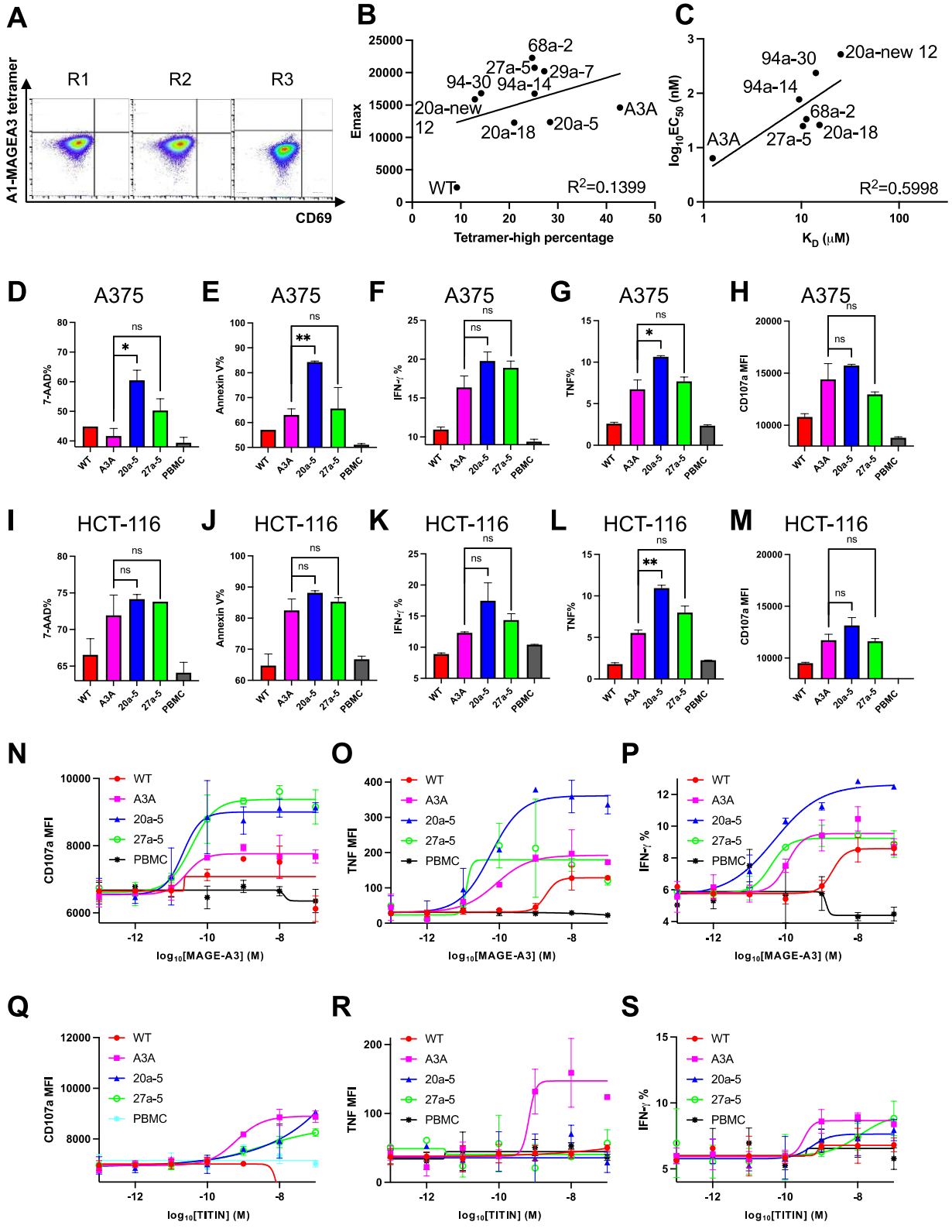

Figure S11. Killing, cytokine responses, and granule release mediated by other MAGE-A3-specific TCR mutants.

(A) A1-MAGE-A3 tetramer staining and anti-CD69 staining of MAGE-A3 WT TCR SKW3 transfectants in each round of selection of the library.

(B) The correlation between E_{max} and percentage of HLA-A1-MAGE-A3 tetramer staining-high population of different MAGE-A3-specific TCR mutants in SKW3 cells.

(C) The correlation between $\log_{10}EC_{50}$ and 3D binding affinity K_D of selected MAGE-A3-specific TCR mutants binding to HLA-A1-MAGE-A3.

(D-E) Killing of A375 melanoma cell line by different MAGE-A3-specific TCR transduced human primary T cells.

(F-H) IFN-γ, TNF, and cytotoxic granule release (CD107a staining) by different MAGE-A3-specific TCR transduced human primary T cells stimulated by the A375 melanoma cell line

(I-J) Killing of HCT-116 colon cancer cell line by different MAGE-A3-specific TCR transduced human primary T cells.

(K-M) IFN-γ, TNF, and cytotoxic granule release (CD107a staining) by different MAGE-A3-specific TCR transduced human primary T cells, stimulated by the HCT-116 colon cancer cell line.

(N-P) Cytotoxic granule release (CD107a staining), TNF, and IFN-γ by different MAGE-A3-specific TCR transduced human primary T cells, stimulated by HLA-$A1^+$ 293T cells pulsed with titrated MAGE-A3 peptide.

(Q-S) Cytotoxic granule release (CD107a staining), TNF, and IFN-γ by different MAGE-A3-specific TCR transduced human primary T cells, stimulated by HLA-$A1^+$ 293T cells pulsed with titrated TITIN peptide.

(D-S) Data are representative of 3 independent experiments. Data are shown as mean ± SD of technical duplicates. ns: not significant; ∗: P<0.05; ∗∗: P<0.01; ∗∗∗: P<0.001; ∗∗∗∗: P<0.0001

Supplementary Figure 12

A

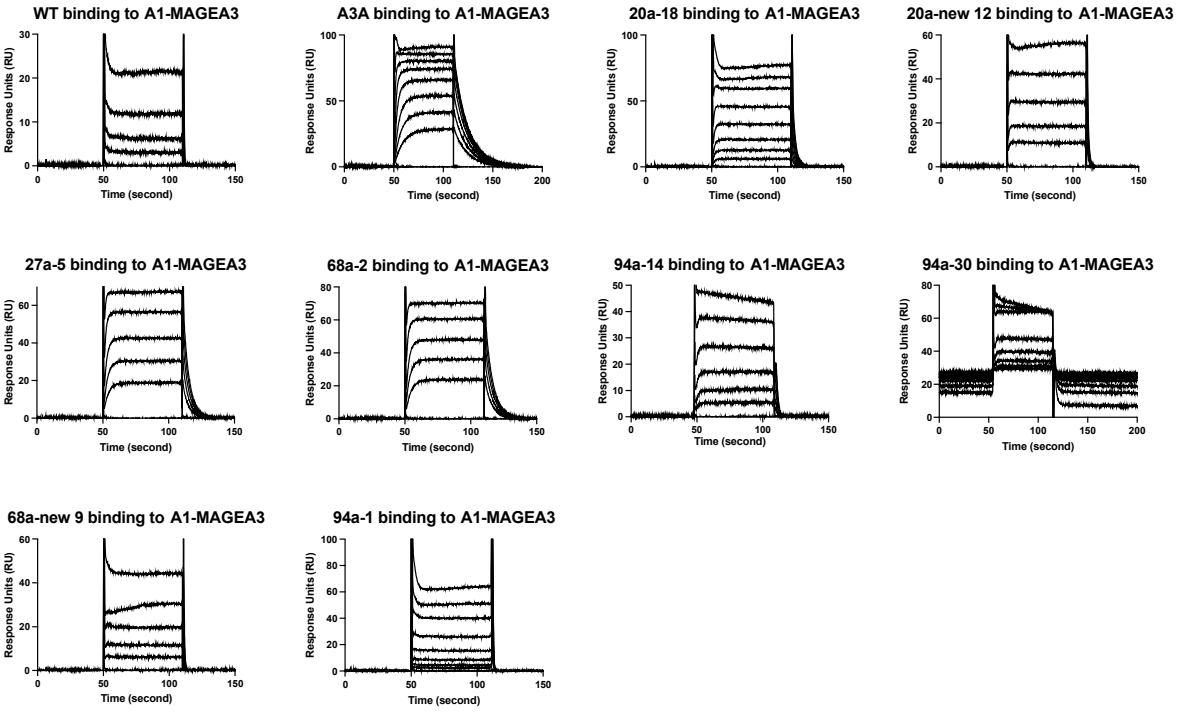

B

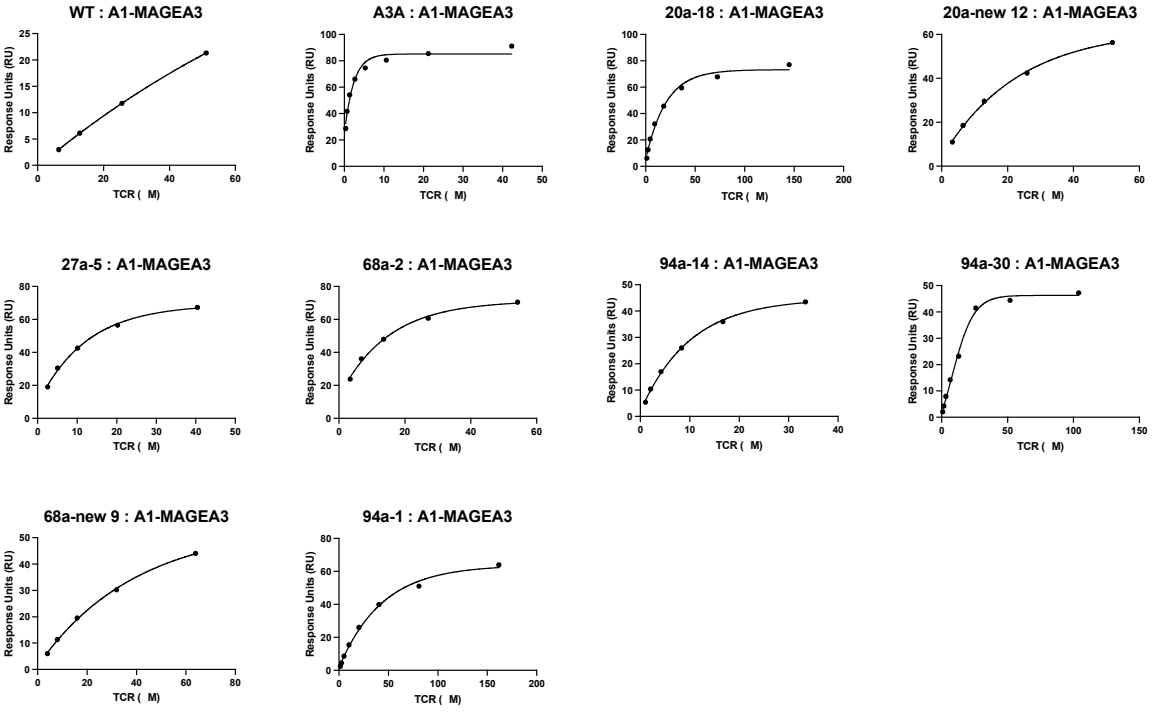

Figure S12. SPR experiments of MAGE-A3-specific TCR mutants binding to HLA-A1-MAGE-A3.

(A) SPR experiments of MAGE-A3-specific TCR mutants protein binding to HLA-A1-MAGE-A3. Biotinylated HLA-A1-MAGE-A3 monomer was immobilized on the streptavidin chip and the MAGE-A3-specific TCR mutant proteins were flowed through the chip.

(B) Determination of 3D affinity between MAGE-A3-specific TCR mutants and HLA-A1-MAGE-A3 by SPR. Equilibrium curves of MAGE-A3-specific TCR mutants binding to HLA-A1-MAGE-A3 pMHC at 25°C. Data shown was measured at equilibrium (black dots). Black lines show the fit to a 1:1 binding curve.

Supplementary Figure 13

A

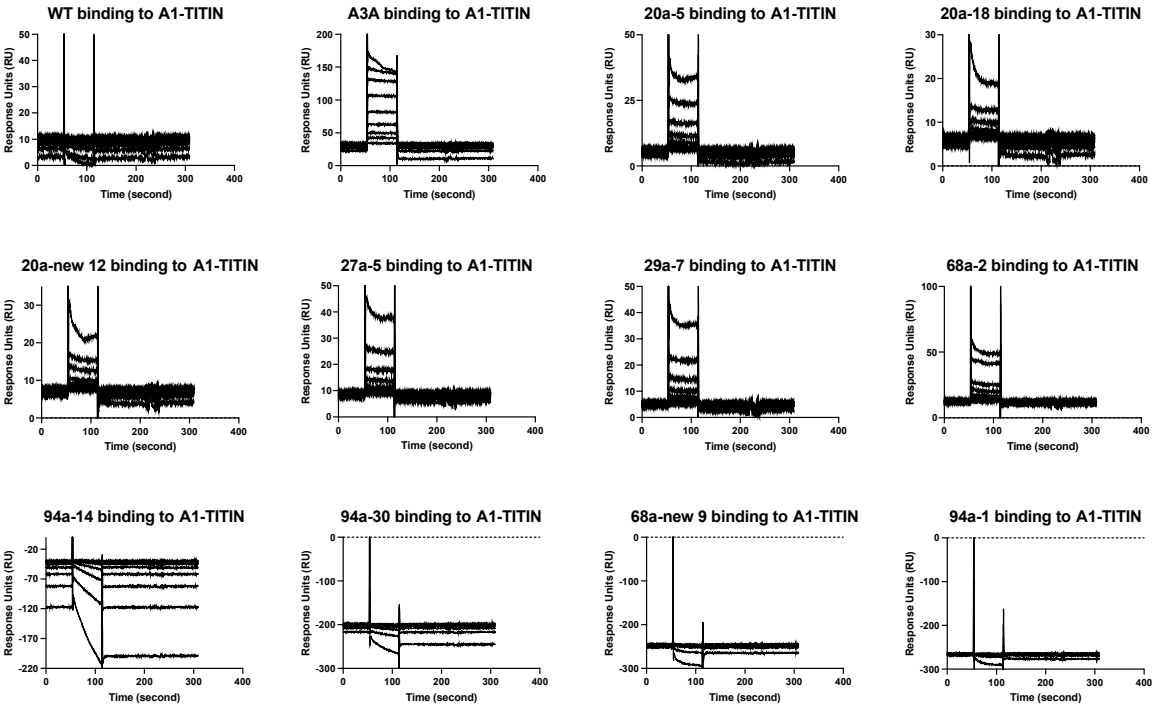

B

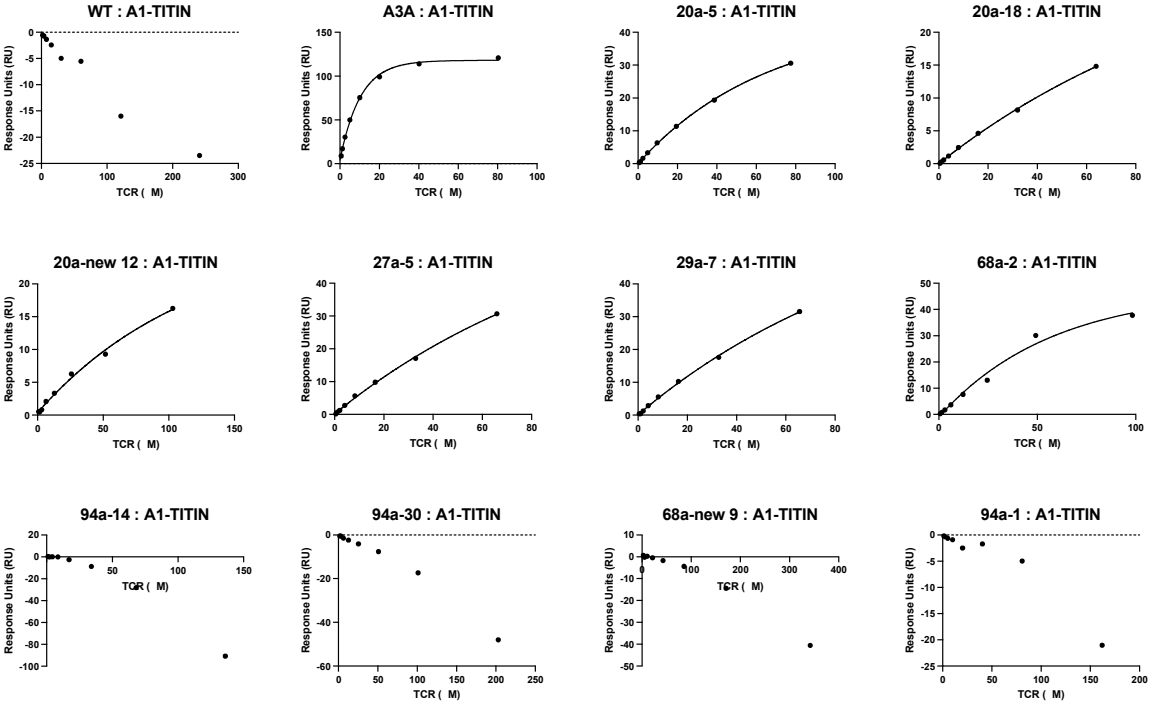

Figure S13. SPR experiments of MAGE-A3-specific TCR mutants binding to HLA-A1-TITIN.

(A) SPR experiments of MAGE-A3-specific TCR mutants protein binding to HLA-A1-TITIN. Biotinylated HLA-A1-TITIN monomer was immobilized on the streptavidin chip and the MAGE-A3-specific TCR mutant proteins were flowed through the chip.

(B) Determination of 3D affinity between MAGE-A3-specific TCR mutants and HLA-A1-TITIN by SPR. Equilibrium curves of MAGE-A3-specific TCR mutants binding to HLA-A1-TITIN pMHC at 25°C. Data shown was measured at equilibrium (black dots). Black lines show the fit to a 1:1 binding curve.

Supplementary Figure 14

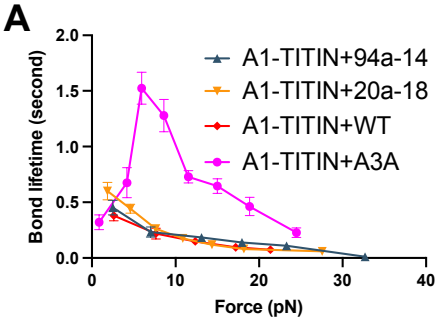

Figure S14. Biomembrane force probe experiments to measure bond lifetime force curves for 94a-14 TCR or 20a-18 TCR binding to A1-TITIN. Data are shown as mean ± SEM of 500+ individual bond lifetimes per force curve.

Supplementary Figure 15

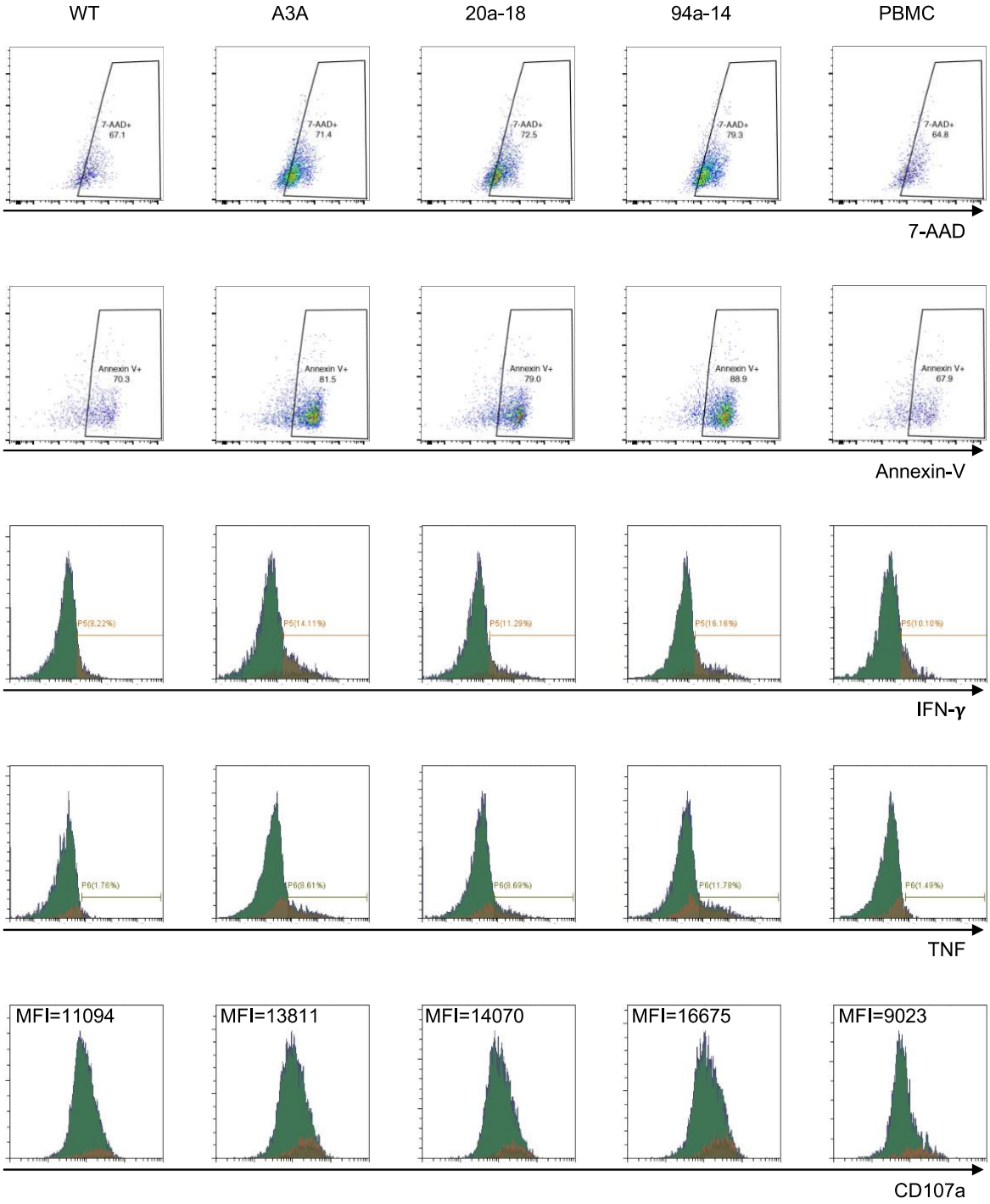

Figure S15. Representative flow cytometry plots of Figure 5F-5J.

Supplementary Figure 16

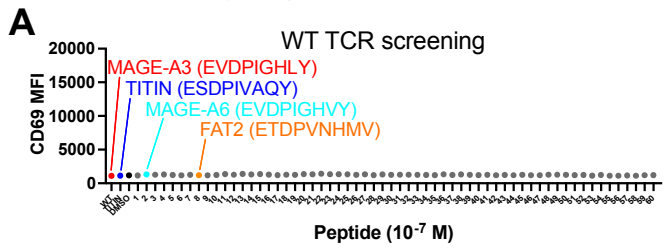

Figure S16. MAGE-A3 (red dot), TITIN (blue dot), DMSO (black dot) and 60 predicted peptides (MAGE-A6: cyan dot; FAT2: orange dot) were used to pulse 293T-HLA-A1 cells to stimulate SKW3 T cells expressing WT MAGE-A3 TCR for 14 hours. Anti-CD69-APC staining was performed and analyzed on flow cytometry. Data are representative of 2 independent experiments.

Table S1 3D affinity and EC_{50} of TCR55α-A98 mutants

TCR	A98H	A98D	A98E	A98F	A98Q	A98Y	WT	A98N	A98S	A98T	A98K	A98R	A98C	A98W
3D K_D (μM)	5.89	3.14	3.37	5.36	8.04	3.36	19.96	9.971	12.26	8.447	8.503	15.49	11.5	6.502
EC_{50} (μM)	2.801	3.174	1.594	2.07	1.59	1.724	2758	3452	2.43	3.332	5.384	0.01	0.044	1.722

Table S2 3D affinity and EC_{50} of TCR55β-A50 mutants

TCR	A50D	A50E	A50F	A50H	A50N	A50Q	A50S	A50T	A50Y	WT	A50C	A50K	A50R	A50W
3D K_D (μM)	2.429	2.238	11.11	5.222	11.41	8.378	10.68	7.834	6.761	19.96	21.11	22.42	17.6	18.29
EC_{50} (μM)	6.169	4.695	8.521	6.306	19.85	6.535	23.17	4.98	18.33	4046	0.9349	0.1622	>1000	6.599

Table S3 Mean values of single-cell AUC distributions

	MAPK-KTR Reporters		Split-GFP Reporters
Stimulation Type	ERK	p38	NFAT2
HIVpol (TCR55)	0.05	5.92	-11.5
HIVpol (TCR55α-A98H)	100.15	15.96	66.55
HIVpol (TCR55β-A50E)	129.22	26.00	125.94
HIVpol (TCR589)	155.47	29.55	181.36

Table S4 Mean values of single-cell AUC distributions (basal corrected & normalized)

	MAPK-KTR Reporters		Split-GFP Reporters
Stimulation Type	ERK	p38	NFAT2
HIVpol (TCR55)	0%	0%	0%
HIVpol (TCR55α-A98H)	64.4%	42.5%	40.5%
HIVpol (TCR55β-A50E)	83.1%	85%	71.3%
HIVpol (TCR589)	100%	100%	100%

Table S5 Specific amino acid mutations of each MAGE-A3 TCR mutants

	TCR α chain position	28	30	51	52	53	54
TCR							
WT		D	A	I	Q	S	S
A3A		D	A	V	R	P	Y
20a-18		H	H	I	R	S	N
20a-5		G	H	I	R	S	N
20a-new 12		H	H	I	R	S	R
27a-5		G	H	I	R	S	E
29a-7		G	H	I	R	S	D
68a-2		N	H	I	R	S	D
94a-14		G	S	I	R	S	S
94a-30		K	E	I	R	S	S
68a-38		K	N	I	R	S	D
68a-new 9		N	H	I	Q	S	H
94a-1		H	H	I	H	S	H
94a-10		S	G	I	R	S	D
94a-19		N	G	I	R	S	S

Table S6 3D affinity and EC_{50} of MAGE-A3 TCR mutants binding to HLA-A1-MAGE-A3

TCR	WT	A3A	20a-18	20a-new12	27a-5	68a-2	94a-14	94a-30	68a-new9	94a-1
3D K_D (μM)	193.3	1.241	15.38	25.36	10.4	11.27	9.512	14.11	50.78	42.3
EC_{50} (nM)	1.302	6.365	26.11	519.6	24.87	33.49	77	236.3	380.5	569.5

Table S7 3D affinity of MAGE-A3 TCR mutants binding to HLA-A1-TITIN

TCR	WT	A3A	20a-5	20a-18	20a-new12	27a-5	29a-7	68a-2	94a-14	94a-30	68a-new 9	94a-1
3D K_D (μM)	N.M.	7.726	98.79	207.4	185.3	186.8	182.6	83.5	N.M.	N.M.	N.M.	N.M.

N.M.: not measurable

Table S8 Top 35 predicted wild-type peptides for TCR A3A.

Ranking	Name	Sequence	Prediction score
1	TTN	ESDPIVAQY	23.73
2	WDR64	EEDPIASQL	19.46
3	EIF3E	ETEPIVKMF	19.20
4	ANAPC1 TSG24	ETEPIVPEL	19.14
5	CYTH4	ERDPINLQV	19.13
6	REV3L POLZ REV3	EFDPICALF	18.81
7	MAGEA3	EVDPIGHLY	18.57
8	DOCK7	EIEPIFASL	18.56
9	ZNF512 hCG_1784442	EQEPVPAQF	18.35
10	BCL2L2	EMEPLVGQV	18.32
11	TTN	DSDPVVAQI	18.24
12	PREX2 DEPDC2	EEEPLVANV	18.19
13	ZDBF2	ENEPIDSEV	18.10
14	MAGEA6 MAGE6	EVDPIGHVY	17.96
15	ANK2	ESEPELAQL	17.77
16	MAGEB18	EVDPIRHYY	17.76
17	JPH4 JPHL1 KIAA1831	EPEPIAMLV	17.54
18	PLEKHJ1 GNRPX	EAEPVGALL	17.43
19	KCNC4 C1orf30	ETEPILTYI	17.38
20	CENPF	ESEPIRNSV	17.35
21	PCDH18 KIAA1562	EGDPIDTFV	17.3450935
22	FAT4 CDHF14 FATJ Nbla00548	EGEPIGTNV	17.3226175
23	PDZRN3 KIAA1095 LNX3	AKEPIVVQV	17.3032435
24	MAP1B	ETEPVEAYV	17.2988336
25	TSTA3	EVEPIILSV	17.2284022
26	CDH23 KIAA1774 KIAA1812	ENEPSVTQL	17.2250452
27	MYBL2 BMYB	EQEPIGTDL	17.2095391
28	MLLT6 AF17	TMEPIVLQY	17.1979566
29	COG4	ELDPILTEV	17.174741
30	ATP5PF	ELDPIQKLF	17.1714644
31	VSIG1 GPA34	EMEPISIYF	17.1686524
32	PIM1	EKEPLESQY	17.1436207
33	MED13 ARC250 KIAA0593	EEDPILSSF	17.1359861
34	PDGFB PDGF2 SIS	EGDPIPEEL	17.1352707
35	CFAP54	ETEPMVLLL	17.119691

Table S9 Top 35 predicted wild-type peptides for TCR 94a-14.

Ranking	Name	Sequence	Prediction score
1	MAGEA3 MAGE3	EVDPIGHLY	16.81
2	MAGEA6 MAGE6	EVDPIGHVY	16.10
3	ZDBF2 KIAA1571	ENEPIDSEV	15.78
4	SNX29 RUNDC2A	ETEPVFWYY	15.65
5	MAGEB18	EVDPIRHYY	15.62
6	FCER1A FCE1A	ESEPVYLEV	15.51
7	C11orf16	NTDPIFLEM	15.27
8	FBXO41 FBX41 KIAA1940	ATDPVGHEV	15.24
9	CDHR1 KIAA1775 PCDH21 PRCAD	EGDPISYHI	15.12
10	FAT2 CDHF8 KIAA0811 MEGF1	ETDPVNHMV	15.02
11	ARSD	DSEPLYHAV	15.01
12	ANKRD30B	SVEPIFSLF	15.00
13	ANAPC1 TSG24	ETEPIVPEL	14.98
14	RAB3IL1	DAEPMFWEI	14.89
15	DCHS2	SSEPIFYRI	14.89
16	PDE12	ESDPLHKEL	14.87
17	NYAP2 KIAA1486	EEEPVYIEM	14.79
18	SPIDR	DEDPIYKLY	14.77
19	MAGEE1 HCA1 KIAA1587	DSDPVQYEF	14.74
20	MYO16 KIAA0865 MYO16B NYAP3	DSEPVYIEM	14.70
21	PIK3C2A	STEPIYLSL	14.6732437
22	SLC13A4 SUT1	EAEPISLDV	14.6705914
23	GNL3L	DTDPLEMEI	14.6357622
24	ELP1 IKAP IKBKAP	EVDPVSREV	14.6339629
25	UNC5C	EQEPLGKEV	14.6338296
26	FAM217B C20orf177	EIDPVYFDL	14.6317501
27	USP26	EKEPLAHLM	14.6015921
28	COG4	ELDPILTEV	14.5888571
29	MYBL2 BMYB	EQEPIGTDL	14.5673226
30	PDGFB PDGF2 SIS	EGDPIPEEL	14.5337701
31	ACER3	VKEPIFHQV	14.5006386
32	STAG1 DKFZp781D1416	DAEPIFEDV	14.4719977
33	MERTK	VSDPIYIEV	14.4641397
34	DISP3 KIAA1337 PTCHD2	EEEPVSLEL	14.458422
35	PPP2R5C KIAA0044	ITEPIYPEV	14.4560187

Table S10 Top 35 predicted wild-type peptides for TCR 20a-18.

Ranking	Name	Sequence	Prediction score
1	SNX29 RUNDC2A	ETEPVFWYY	17.26
2	MAGEA3	EVDPIGHLY	16.47
3	RAB3IL1	DAEPMFWEI	16.12
4	C11orf16	NTDPIFLEM	15.80
5	PIK3C2A	STEPIYLSL	15.75
6	FBXO41 FBX41 KIAA1940	ATDPVGHEV	15.70
7	ZDHHC16	AFEPVYWLV	15.62
8	MAGEA6	EVDPIGHVY	15.59
9	FCER1A FCE1A	ESEPVYLEV	15.51
10	ANKRD30B	SVEPIFSLF	15.46
11	RAB3IL1	LTEPMFWEI	15.42
12	NWD1	TAEPVFHIL	15.42
13	ACER3	VKEPIFHQV	15.30
14	FAT2 CDHF8 KIAA0811 MEGF1	ETDPVNHMV	15.24
15	SPIDR	DEDPIYKLY	15.24
16	MAGEB18	EVDPIRHYY	15.21
17	DCHS2	SSEPIFYRI	15.17
18	ARSD	DSEPLYHAV	15.11
19	MYO16 KIAA0865 MYO16B NYAP3	DSEPVYIEM	15.05
20	NYAP2 KIAA1486	EEEPVYIEM	14.93
21	GPR82	STDPIIFLL	14.82447
22	NUFIP1	RKEPVFHFF	14.816694
23	FAT3 CDHF15 KIAA1989	TSEPIYYPV	14.807425
24	PPP2R5C	ITEPIYPEV	14.7779635
25	CSMD3 KIAA1894	QTEPIYDFI	14.7775383
26	FAM217B C20orf177	EIDPVYFDL	14.7767125
27	DNAH17	DKEPVPWEF	14.7310013
28	SLC3A1	EVDPIFGTM	14.717045
29	NOMO1	KIEPVFHVM	14.6294235
30	MFSD2A MFSD2 NLS1 HMFN0656	GTEPIFFSF	14.6004367
31	ELP2 STATIP1	EFEPVFSLF	14.5157106
32	STAG1 SA1 SCC3	DAEPIFEDV	14.494468
33	MGA KIAA0518 MAD5	DKDPVYLYF	14.474143
34	DOCK6 KIAA1395	EIEPIFGIL	14.4357737
35	FAT1 CDHF7 FAT	ESDPVAHMI	14.4343329

Table S11 Top 35 predicted wild-type peptides for TCR 94a-30.

Ranking	Name	Sequence	Prediction score
1	RAB3IL1	DAEPMFWEI	20.0667597
2	SPIDR KIAA0146	DEDPIYKLY	19.5092452
3	DNAH17	DKEPVPWEF	19.4827738
4	CUX1 CUTL1	REEPIEWEF	19.143669
5	MYO16	DSEPVYIEM	18.6962277
6	SHMT2	DSDPEMWEL	18.423906
7	CCDC146 KIAA1505	DQEPIYAIV	18.4129163
8	PPP2R5C	ITEPIYPEV	18.3599013
9	MUC16	DREQLYWEL	18.2302094
10	MUC16 CA125	DRERLYWEL	18.1688925
11	GVINP1 GVIN1 VLIG1	DSENILWEY	17.7209221
12	MERTK	VSDPIYIEV	17.6664431
13	ROS1 MCF3 ROS	DGDLIYWII	17.4945727
14	FCER1A FCE1A	ESEPVYLEV	17.3626517
15	SNTA1 SNT1	DPEPRYLEI	17.3616783
16	ANAPC1 TSG24	ETEPIVPEL	17.3228682
17	ZP4 ZPB	LRDPIYVEV	17.2909522
18	GPR151 GALR4 GALRL PGR7	DNDPIPWEH	17.1894581
19	C11orf16	NTDPIFLEM	17.1560792
20	ARSD	DSEPLYHAV	17.0613837
21	ZDHHC16	AFEPVYWLV	17.0503827
22	NYAP2 KIAA1486	EEEPVYIEM	16.9569564
23	PIK3C2A	STEPIYLSL	16.9116585
24	NYNRIN CGIN1 KIAA1305	LTEPLWWEM	16.9105401
25	GSTA3	RMEPIRWLL	16.9103569
26	RAB3IL1	LTEPMFWEI	16.8881982
27	SNX29 RUNDC2A	ETEPVFWYY	16.8561948
28	FXYD2 ATP1C ATP1G1	DVDPFYYDY	16.8540202
29	ZDBF2	ENEPIDSEV	16.7988416
30	MAGEE1 HCA1 KIAA1587	DSDPVQYEF	16.7847655
31	LAMA2 LAMM	HLEPFYWKL	16.7546725
32	DNAH17	ETEGIPWEV	16.7150722
33	COG4	ELDPILTEV	16.6944252
34	MAGEA3 MAGE3	EVDPIGHLY	16.6913823
35	TRIM27 RFP RNF76	EREKIVWEF	16.6573062

Table S12 60 wild-type peptides tested for activation.

Peptide ID	Peptide name	Peptide sequence
1	ZDBF2 KIAA1571	ENEPIDSEV
2	MAGEA6 MAGE6	EVDPIGHVY
3	MAGEB18	EVDPIRHYY
4	ANAPC1 TSG24	ETEPIVPEL
5	WDR64	EEDPIASQL
6	PCDH18 KIAA1562	EGDPIDTFV
7	EIF3E	ETEPIVKMF
8	FAT2 CDHF8 KIAA0811 MEGF1	ETDPVNHMV
9	PDGFB PDGF2 SIS	EGDPIPEEL
10	CYTH4 CYT4 PSCD4	ERDPINLQV
11	DOCK7 KIAA1771	EIEPIFASL
12	CDHR1 KIAA1775 PCDH21 PRCAD	EGDPISYHI
13	SNX29 RUNDC2A	ETEPVFWYY
14	JPH4	EPEPIAMLV
15	KCNC4 C1orf30	ETEPILTYI
16	MYBL2 BMYB	EQEPIGTDL
17	COG4	ELDPILTEV
18	CFAP44 WDR52	ETEPIPEDI
19	FCER1A	ESEPVYLEV
20	VSIG1 GPA34	EMEPISIYF
21	RAB3IL1	DAEPMFWEI
22	C11orf16	NTDPIFLEM
23	PIK3C2A	STEPIYLSL
24	FBXO41 FBX41 KIAA1940	ATDPVGHEV
25	ZDHHC16	AFEPVYWLV
26	ANKRD30B	SVEPIFSLF
27	RAB3IL1	LTEPMFWEI
28	NWD1	TAEPVFHIL
29	ACER3	VKEPIFHQV
30	SPIDR	DEDPIYKLY
31	DCHS2	SSEPIFYRI
32	ARSD	DSEPLYHAV
33	MYO16 KIAA0865 MYO16B NYAP3	DSEPVYIEM
34	NYAP2 KIAA1486	EEEPVYIEM
35	GPR82	STDPIIFLL
36	ELP1 IKAP IKBKAP	EVDPVSREV
37	UNC5C	EQEPLGKEV
38	PDE12	ESDPLHKEL
39	P3H2 LEPREL1 MLAT4	TLDPLYREL
40	TEX14 SGK307	SVEPVSSEI
41	PNKD KIAA1184 MR1 TAHCCP2 FKSG19 UNQ2491/PRO5778	EPEPLSPEL
42	HINFP MIZF ZNF743	EDDPLEEEF
43	A2M CPAMD5 FWP007	HLEPMSHEL
44	ZNF280D KIAA1584 SUHW4 ZNF634	EQEPVSKEI
45	PPP2R5C	ITEPIYPEV
46	MCM3AP GANP KIAA0572 MAP80	QEEPLPHEL
47	MAGEE1 HCA1 KIAA1587	DSDPVQYEF
48	DNAH17	DKEPVPWEF
49	CUX1 CUTL1	REEPIEWEF
50	SHMT2	DSDPEMWEL
51	CCDC146 KIAA1505	DQEPIYAIV
52	MUC16	DREQLYWEL
53	MUC16 CA125	DRERLYWEL
54	GVINP1 GVIN1 VLIG1	DSENILWEY
55	MERTK	VSDPIYIEV
56	ROS1 MCF3 ROS	DGDLIYWII
57	SNTA1 SNT1	DPEPRYLEI
58	ZP4 ZPB	LRDPIYVEV
59	GPR151 GALR4 GALRL PGR7	DNDPIPWEH
60	MAGE-A12	EVVRIGHLY